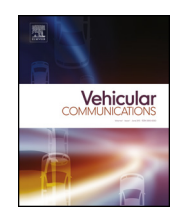
ELSEVIER

Contents lists available at ScienceDirect

Vehicular Communications

www.elsevier.com/locate/vehcom



Optimized modulation order for V2V communication over index-modulated radar signals *



Mai Kafafy ^{a,*}, Ahmed S. Ibrahim ^b, Mahmoud H. Ismail ^{c,a}

- ^a Electronics and Communications Engineering Department, Cairo University, Giza, 12613, Egypt
- ^b Electrical and Computer Engineering Department, Florida International University, Miami, 33174, FL, USA
- ^c Department of Electrical Engineering, American University of Sharjah, Sharjah, PO Box 26666, United Arab Emirates

ARTICLE INFO

Article history: Received 15 December 2021 Received in revised form 4 March 2022 Accepted 31 May 2022 Available online 2 June 2022

Keywords:
Spectrum sharing
Dual function
Radar
Vehicular communications
Index modulation

ABSTRACT

Embedding information messages in radar signals through index modulation is a promising approach for dual function radar and communication in automotive systems. In this paper, we optimize the index modulation order to maximize the communication performance without compromising the radar operation. We derive novel expressions for the number of successfully transmitted bits per symbol and the target detection probability as functions of the road layout, traffic conditions and index modulation order. Results show that in light traffic conditions, index modulation can achieve up to 12 bits/symbol when line of sight is present between the transmit and receive vehicles with up to 140% improvement compared to the case with absent line of sight. Finally, we show that the received radar signal can be used, at the receive vehicle, to estimate the location of the transmitting vehicle via a maximum-likelihood estimator.

© 2022 Elsevier Inc. All rights reserved.

1. Introduction

Modern vehicles are equipped with radar sensors to provide comfortable safe trips and reduce the number of road accidents. The benefits of radar sensors include detecting other vehicles, pedestrians, and available parking spaces, measuring inter-vehicle distance and warning drivers in case of potential collision, assisting drivers when changing lanes, etc. Even in the presence of LiDar/ViLDar systems, conventional radar sensors are still important especially in rainy or foggy weather when the propagation of optical signals is hindered [1]. In addition, vehicles communicate with their neighbors for different purposes including entertainment, traffic information, safety warnings, etc. Traditionally, communication and radar are regarded as two different functions that are performed by two different systems on different bands. Albeit, recently, the research community has shown growing interest in combining the two functions in one system, which is known as Dual Function Radar Communication (DFRC). This combining has numerous advantages including power saving, cost reduction, and

E-mail addresses: mai.b.s.ali@eng.cu.edu.eg (M. Kafafy), aibrahim@fiu.edu (A.S. Ibrahim), mhibrahim@aus.edu (M.H. Ismail).

better utilization of the Radio Frequency (RF) spectrum [2,3]. This is particularly important for vehicular systems where increased power consumption, interference, and spectrum congestion can be problematic especially in urban areas with dense vehicle traffic. Besides, providing affordable smart vehicles is essential to establish intelligent transportation systems.

One approach to DFRC is the coordinated transmission of different radar and communication waveforms using time division [4], frequency division [5], or antenna division [6]. However, this division results in an inevitable waste of resources. To overcome the aforementioned waste, another interesting DFRC approach suggests using the radar waveform for concurrent radar sensing and communication by embedding information in the radar waveform using Index Modulation (IM) [3]. This approach does not require designing new radar waveforms as IM encodes data symbols in the selected indices of transmission parameter(s) such as sub-carriers, time slots, etc [7]. Consequently it allows using the radar resources for concurrent radar sensing and communication with minimal effect on the radar operation. This, in turn, facilitates its integration in intelligent transportation systems where vehicles continuously use their radar systems to sense their surroundings.

IM has different schemes that were considered in a large body of communication research. In this paragraph we give a brief overview of the topic, however we refer interested readers to the recent surveys in [7–10] where different IM schemes are discussed and categorized according to their domain(s). IM is a relatively

[☆] This work was supported by the American University of Sharjah under a Faculty Research Grant no. FRG20-M-E10. The work of Ahmed S. Ibrahim was supported in part by the National Science Foundation under Award CNS-1816112.

^{*} Corresponding author.

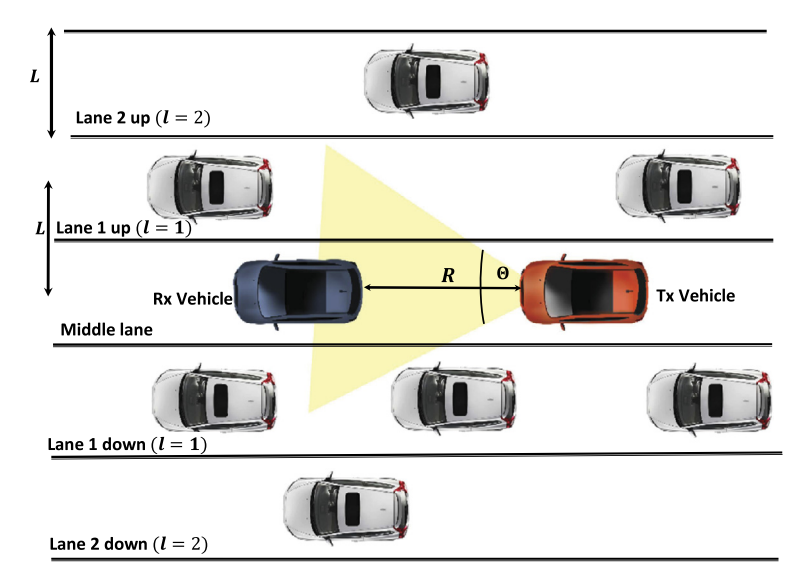


Fig. 1. A typical Tx vehicle uses its radar to detect and communicate with a Rx vehicle ahead of it on a multi-lane road.

new modulation technique that embeds information in the selected indices of one or more transmission parameters in different domains. These domains include space, frequency, code, etc. An example of IM in space domain is the generalized space shift keying which encodes data in the indices of the active transmit antennas. Generalized spatial modulation and Orthogonal Frequency Division Multiplexing with Index Modulation (OFDM-IM) are two famous early modulation schemes that combine traditional modulation (e.g. amplitude and phase) with IM in the space domain and frequency domain, respectively. In these techniques, part of the data is encoded in the indices of the active antennas (or subcarriers) and the other part is encoded using traditional modulation over the selected antennas (or sub-carriers) [8]. Afterwards, the use of IM extended to include more transmission parameters such as antenna beam patterns, elements of re-configurable intelligent surfaces, space-time dispersion matrices, spread codes, polarization states, RF mirrors, etc. References [11-13] used IM to encode data in the radar waveform. Specifically, [11] encodes data in the permutations of multiple orthogonal waveforms over the transmit antennas. In [12], only a subset of the transmit antennas is active and data is encoded in the indices of the active antennas and the permutation of the waveforms over them. Finally, [13], encodes the data in the different permutations of hopping codes.

In this paper, we consider an IM-based DFRC scenario where data is embedded in the sub-carriers selection of a multi-carrier frequency agile radar. Apparently, the number of selected sub-carriers affects both the communication data rate and the radar performance of the vehicle. Consequently, our purpose is optimizing the modulation order of the index modulated signal to maximize data transmission without harming the radar operation. This approach is different from the other discussed works in literature as these works mainly focused on the signal processing between a single transmitter and receiver without optimizing the modulation order of the transmission or considering interference from other transmitters. The novelty of our work is summarized as follows:

- Optimizing the modulation order to maximize the number of successfully transmitted bits/symbol between a transmit and receive vehicle subject to a constraint on the target detection probability at the transmit vehicle. The optimization does not require instantaneous CSI at the transmit or receive vehicle.
- Deriving novel expressions for the number of successfully transmitted bits/symbol between the transmit and receive vehicles and the target detection probability at the transmit ve-

- hicle as functions of the road layout, the traffic conditions, and the IM order in the two cases of LoS and Non-LoS (NLoS).
- Showing through analysis that sub-carrier IM and energy detection based demodulation promote an additional use of the radar signal such that the receive vehicle can use the Received Signal Strength (RSS) of the transmit vehicle radar signal not only to decode the embedded data, but also to estimate the distance between itself and the transmit vehicle. This additional use of the transmit vehicle radar signal should save more power and spectrum.

Numerical results show that IM can achieve up to 12 bits/symbol LoS communication to distances up to 20 m in light traffic conditions without jeopardizing the radar detection. The absence of LoS reduces the communication to around 5 bits/symbol.

The rest of this paper is organized as follows: the system model and statistical characterization of the transmission signals are presented in Sections 2 and 3, respectively. The optimization problem is formulated and solved in Sections 4 and 5, respectively, and the RSS-based distance estimation at the receive vehicle is proposed in Section 6. Numerical results are presented in Section 7, and finally the paper is concluded in Section 8.

2. System model

We consider vehicles on a multi-lane road as shown in Fig. 1. At a taken snapshot of the road, the vehicles positions in any lane are modeled as a one dimensional Homogeneous Poisson Point Process (HPPP) [14]. Vehicles are equipped with frequency agile multi-carrier radars on their front ends and with communication receivers on their rear ends. P_{tx} and Θ denote, respectively, the transmission power and beamwidth of the radar, and Ψ denotes the total number of radar sub-carriers. We consider, without loss of generality, typical transmit (Tx) and receive (Rx) vehicles in the middle lane as shown in Fig. 1. The two vehicles are separated by distance R. The Tx vehicle uses its radar signal to detect and communicate information to the Rx vehicle.

The considered IM based DFRC consists of two parts: one at the Tx vehicle and the other at the Rx vehicle. The Tx vehicle transmits its radar signal over ψ sub-carriers, and it uses the received reflected signal over these sub-carriers for ordinary radar operation. The Tx vehicle also encodes data symbols in the indices of the selected sub-carriers, and consequently the number of transmitted bits per symbol is determined by ψ . When the Tx vehicle trans-

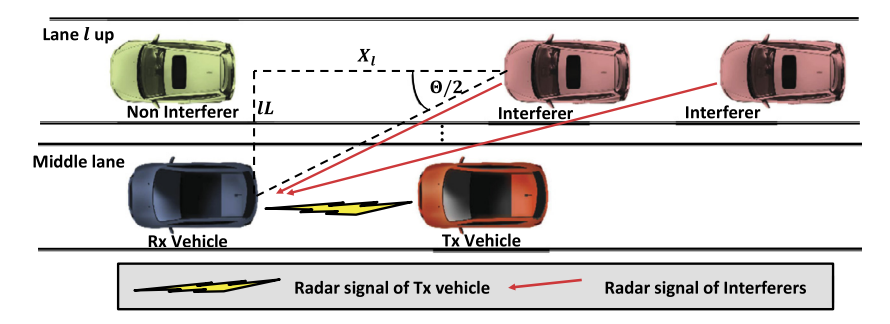


Fig. 2. The signal received at Rx vehicle from the Tx vehicle and a general interfering lane l.

mits over a set of ψ sub-carriers out of the total Ψ sub-carriers, then the number of symbols in the constellation (i.e., the modulation order) is $\binom{\Psi}{\psi}$, where (;) is the combination operator, and the Tx vehicle can transmit $\log_2\binom{\Psi}{\psi}$ bits/symbol. To decode the data symbols, the Rx vehicle needs to determine the indices of the sub-carriers used by the Tx vehicle. This is an energy detection based binary hypothesis test per sub-carrier. The Rx vehicle detects the received signals over the different sub-carriers and decides which sub-carriers were used. The Rx vehicle can also use the RSS over the used sub-carriers to estimate the distance between the Tx vehicle and itself.

The benefits of the procedure are summarized as follows:

- The simultaneous use of the same signal for radar sensing and data communication should reduce power consumption and hardware costs and allow better utilization of the RF spectrum.
- sub-carrier IM requires simple energy detection at the Rx vehicle to decode the data symbols, and consequently cheap communication receivers can be used.
- The procedure does not require instantaneous CSI at the transmit or receive vehicle. This feature significantly reduces the required control message exchange between the Tx and Rx vehicle and simplifies its application.

The number of sub-carriers used by the Tx vehicle affects both the radar performance of the Tx vehicle and its communication data rate with the Rx vehicle. Consequently, in the rest of this paper we optimize the number of the sub-carriers that should be used by the Tx vehicle to maximize its successfully transmitted bits/symbol to the Rx vehicle without affecting the target detection probability of its (the Tx vehicle) radar.

3. Statistical characterization of signal transmission between Tx and Rx vehicles

In this section, we statistically characterize the radar signal received at the Rx vehicle and the received reflected radar signal at the Tx vehicle.

3.1. Received radar signal at the Rx vehicle

The signal received at the Rx vehicle consists of the radar signal from the Tx vehicle, the radar signal from interfering vehicles, and a noise component. The set of interfering vehicles in different lanes are modeled as different independent HPPP [14]. Fig. 2 shows the middle lane and a general interfering lane (number l up the middle lane). From the road geometry in Fig. 2, vehicles in l (up or down the middle lane) interfere with the Rx vehicle only if they lag with distance more than $X_l = l \times L / \tan{(\Theta/2)}$ [14], where $l \times L$ is the distance between lane number l and the middle lane. We assume the interference from other vehicles that come behind

the Tx vehicle in the middle lane to be insignificant as their interference is blocked by the body of the Tx vehicle.

The magnitude of the radar signal received by the Rx vehicle on sub-carrier k, denoted by $r_{rx,k}$, is thus given by

$$r_{rx,k} = \begin{cases} |g_{0,k}s_{rx,k} + n_{rx,k} + i_{rx,k}|, & \text{at } P_{tx,k} \neq 0, \\ |n_{rx,k} + i_{rx,k}|, & \text{at } P_{tx,k} = 0, \end{cases}$$
(1)

where $s_{rx,k} = \sqrt{P_{tx,k}\gamma_k R^{-\alpha}}$ with $P_{tx,k}$ being the transmit power of the Tx vehicle over sub-carrier k and α the pathloss exponent. The case $P_{tx,k} \neq 0$ means the Tx vehicle transmits over sub-carrier k, and vice versa. Also, $\gamma_k = G_k A_k / 4\pi$ where G_k and A_k are the transmit gain and the receive effective area of the antenna on sub-carrier k [15]. In addition, $g_{0,k}$ is the channel gain between the Tx and Rx vehicles on sub-carrier k. The term $n_{rx,k}$ represents the additive white Gaussian noise (AWGN) at the Rx vehicle on sub-carrier k such that $n_{rx,k} \sim \mathcal{CN}(0, \sigma_n^2)$, $\forall k$ are independent and identically distributed (i.i.d.). Finally, the term $i_{rx,k}$ is the interference received at Rx vehicle on sub-carrier k given by

$$i_{rx,k} = \sum_{l_{up,down}} \sum_{i \in \Phi_l} h_{i,k} \sqrt{P_{i,k} \gamma d_i^{-\alpha}}.$$
 (2)

The first summation in (2) is over the interfering lanes on the road and Φ_l is the set of interfering vehicles in lane l. Φ_l is assumed to follow a HPPP with density ζ and i.i.d. marks $P_{i,k}$, where $P_{i,k}$ is the transmit power of interferer $i \in \Phi_l$ on sub-carrier k. Also, $h_{i,k}$ is the small scale channel on sub-carrier k between interferer $i \in \Phi_l$ and the Rx vehicle. Finally, d_i is the distance between interferer $i \in \Phi_l$ and the Rx vehicle. We assume Rayleigh fading between the Rx vehicle and the interfering vehicles such that $h_{i,k} \sim \mathcal{CN}(0,1)$ are i.i.d. We also assume orthogonal sub-carriers such that no interference is present between the different sub-carriers.

Now, if sub-carrier k is not used by the Tx vehicle (i.e., $P_{tx,k} = 0$), then from (1), $r_{rx,k}$ only consists of noise and interference. Therefore, $r_{rx,k}$ follows a Rayleigh distribution as follows

$$f_{r_{rx,k}}(r|P_{tx,k}=0) = \frac{2r}{\sigma_n^2 + \sigma_{rx,k}^2} \exp\left(-\frac{r^2}{\sigma_n^2 + \sigma_{rx,k}^2}\right),$$
 (3)

where σ_n^2 is the noise power and $\sigma_{rx,k}^2$ is interference power at the Rx vehicle on sub-carrier k calculated as follows

$$\sigma_{rx,k}^{2} = \sum_{l} \mathbb{E}_{\Phi_{l},P} \left[\sum_{i \in \Phi_{l}} P_{i,k} \gamma_{k} d_{i}^{-\alpha} \right],$$

$$\stackrel{a}{=} 2\zeta \mathbb{E} \left[P_{k} \right] \sum_{l} \int_{x-l}^{\infty} \frac{\gamma_{k} dx}{\left((lL)^{2} + x^{2} \right)^{\alpha/2}},$$
(4)

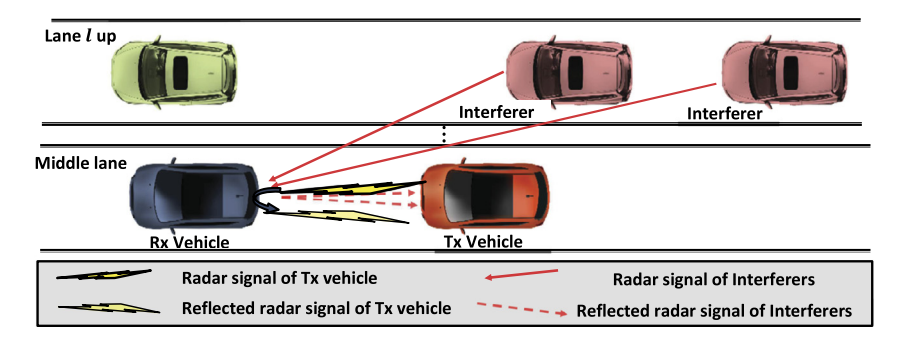


Fig. 3. The Rx vehicle reflects the radar signal of the Tx vehicle and the radar signal of other interfering vehicles back to the Tx vehicle.

where $\mathbb{E}[\cdot]$ is the expectation operator and $\stackrel{a}{=}$ follows from the road geometry in Figs. 1 and 2, the independence of the interferers positions and their marks (i.e., d_i and $P_{i,k}$), and Campbell's theorem [16]. Also, $\mathbb{E}[P_k]$ is the average transmit power over subcarrier k and the factor 2 is to account for the two lanes (up and down lanes) on same distances from the middle lane.

In our analysis, we assume i.i.d. channel conditions over the sub-carriers and the lack of instantaneous CSI at the transmitting/receiving vehicles. We also assume similar antenna performance over the sub-carriers (i.e., equal γ_k). As a result of the preceding assumptions, a typical vehicle i distributes its transmit power equally over its used sub-carriers. Hence, $P_{i,k} \in \left\{0, \frac{P_{1x}}{1}, \frac{P_{tx}}{2}, ..., \frac{P_{tx}}{\Psi}\right\}$ depending on the number of sub-carriers used by vehicle i and on whether sub-carrier k is included in its transmission set or not. Assuming that any vehicle i uses sub-carriers sets of any size from 1 to Ψ with equal probability $1/\Psi$. Then, the probability that a typical interferer i uses sub-carrier k with power $P_{i,k} = P_{tx}/j$ is

$$P\left(P_{i,k} = \frac{P_{tx}}{j}\right)$$

= P(selected set size = i)

 \times P(sub-carrier $k \in$ selected set|selected set size = i),

$$= \frac{1}{\Psi} \times \left(\begin{pmatrix} \Psi \\ j \end{pmatrix} - \begin{pmatrix} \Psi - 1 \\ j \end{pmatrix} \right) / \begin{pmatrix} \Psi \\ j \end{pmatrix} = \frac{j}{\Psi^2}, \tag{5}$$

where $P(\text{sub-carrier } k \in \text{selected set} | \text{selected set size} = j)$ is the probability that sub-carrier k is in the selected set of size j. Since data symbols are equiprobable, then a vehicle selects different sub-carrier sets with equal probability. Therefore, the above probability is calculated as the number of size j subsets that have sub-carrier k divided by the total number of possible size j subsets. The Probability Mass Function (PMF) of the power that a typical vehicle transmits over sub-carrier k is thus

$$P(P_k) = \begin{cases} j/\Psi^2, & \text{at } P_k = P_{tx}/j, \text{ and } j = 1, 2, ...\Psi, \\ (\Psi - 1)/2\Psi, & \text{at } P_k = 0. \end{cases}$$
 (6)

And $\mathbb{E}[P_k]$ in (4) is calculated as follows:

$$\mathbb{E}[P_k] = \sum_{i=1}^{\Psi} \frac{P_{tx}}{j} \times \frac{j}{\Psi^2} = \frac{P_{tx}}{\Psi}.$$
 (7)

Solving the integral in (4) and substituting with $\mathbb{E}[P_k]$ from (7) results in $\sigma_{rx,k}^2$ being equal $\forall k$ and having the following closed forms in the cases $\alpha=2$ and $\alpha=4$:

$$\sigma_{rx}^{2} = \begin{cases} \frac{P_{tx}\gamma\zeta\Theta}{\Psi L} \sum_{l} \frac{1}{l}, & \text{at } \alpha = 2, \\ \frac{P_{tx}\gamma\zeta}{\Psi L^{3}} \left[\frac{\Theta}{2} - \frac{\tan(\Theta/2)}{\tan^{2}(\Theta/2) + 1}\right] \sum_{l} \frac{1}{l^{3}}, & \text{at } \alpha = 4. \end{cases}$$
(8)

So far, the analysis shows that the distribution of $r_{rx,k}$ at $P_{tx,k}=0$ does not depend on the presence of a LoS between the Tx and Rx vehicles. In the rest of this sub-section, we characterize $r_{rx,k}$ at $P_{tx,k}\neq 0$ for the two cases of a LoS and NLoS between the Tx and Rx vehicles.

3.1.1. LoS between Tx and Rx vehicles

In this case, $g_{0,k}=1$, and from (1), $r_{rx,k}$ follows a Ricean distribution as follows

$$f_{r_{rx,k}}(r|P_{tx,k} \neq 0) = \frac{2r}{\sigma_n^2 + \sigma_{rx}^2} \exp\left(-\frac{r^2 + s_{rx,k}^2}{\sigma_n^2 + \sigma_{rx}^2}\right) I_0\left(\frac{2rs_{rx,k}}{\sigma_n^2 + \sigma_{rx}^2}\right), \tag{9}$$

where $I_0(\cdot)$ is the zero order modified Bessel function of the first kind.

3.1.2. NLoS between Tx and Rx vehicles

In this case, we assume a Rayleigh channel between the Tx and Rx vehicles such that $g_{0,k} \sim \mathcal{CN}(0,1)$ are i.i.d. $\forall k$. Consequently, $r_{\text{rx},k}$ follows a Rayleigh distribution as follows

$$f_{r_{rx,k}}(r|P_{tx,k} \neq 0) = \frac{2r}{s_{rx,k}^2 + \sigma_n^2 + \sigma_{rx}^2} \exp\left(-\frac{r^2}{s_{rx,k}^2 + \sigma_n^2 + \sigma_{rx}^2}\right).$$
(10)

3.2. Reflected signal at the Tx vehicle

As shown in Fig. 3, the received reflected signal at the Tx vehicle consists of the radar signal of the Tx vehicle reflected off the Rx vehicle besides the radar signals from other interferers reflected off the Rx vehicle too. The magnitude of the received reflected signal at the Tx vehicle over sub-carrier k, denoted by $r_{tx,k}$, is thus given as follows

$$r_{tx,k} = \left| u_{0,k} \sqrt{\frac{\Omega R^{-\alpha}}{4\pi}} \left(s_{rx,k} + i_{rx,k} \right) + n_{tx,k} \right|,$$
 (11)

where Ω is the radar cross section of the Rx vehicle and $u_{0,k}$ is the channel from the Rx vehicle to the Tx vehicle. The reflections from other vehicles in neighboring lanes reach the Tx vehicle with different delays compared to the signal reflected from the Rx vehicle and therefore, are ignored in the analysis. On the other hand, since the radar transmission of different vehicles is unsynchronized, there is a chance that other radar signals reach the Rx vehicle at the same time as the radar signal of the Tx vehicle and hence, their reflections from the Rx vehicle reach the Tx vehicle overlapped with its own reflected radar signal. Consequently, the reflection of the term $i_{rx,k}$ is considered in the analysis. Just like in the preceding section, we will characterize the distribution of $r_{tx,k}$ in the rest of this subsection.

3.2.1. LoS between Tx and Rx vehicles

Following the analysis in the preceding subsection, when a LoS is present (i.e., $u_{0,k}\approx 1$), $r_{tx,k}$ follows a Ricean distribution as follows

$$f_{r_{tx,k}}(r|P_{tx,k} \neq 0) = \frac{2r}{\sigma_n^2 + \sigma_{tx}^2} \exp\left(-\frac{r^2 + s_{tx,k}^2}{\sigma_n^2 + \sigma_{tx}^2}\right) I_0\left(\frac{2rs_{tx,k}}{\sigma_n^2 + \sigma_{tx}^2}\right),$$
(12)

where $\sigma_{tx}^2 = \Omega R^{-\alpha} \sigma_{tx}^2 / 4\pi$ and $s_{tx,k}^2 = \Omega s_{rx,k}^2 R^{-\alpha} / 4\pi$.

3.2.2. NLoS between Tx and Rx vehicles

In this case, we assume a Rayleigh channel such that $u_{0,k} \sim \mathcal{CN}(0,1)$. The exact Probability Density Function (PDF) of $r_{tx,k}$ in the presence of noise does not have a closed form. Therefore, for simplicity of analysis, we assume that the noise term is negligible compared to the interference term. In this case, the PDF of $r_{tx,k}$ is the PDF of two multiplied independent (but not identically distributed) Rayleigh random variables (RVs). Following the analysis in [17], the PDF of $r_{tx,k}$ is a function of the Meijer-G function as follows

$$f_{r_{tx,k}}(r|P_{tx,k}\neq 0)$$

$$= \frac{1}{2\sqrt{s_{tx,k}^2 + \sigma_{tx}^2}} G_{0,2}^{2,0} \left(\frac{r^2}{s_{tx,k}^2 + \sigma_{tx}^2} \right|_{0.5,0.5}^{-} \right). \tag{13}$$

As discussed in the system model, the Tx vehicle selects random sets (each of size ψ) of sub-carriers to represent different data symbols. The selected set size (i.e., modulation order) affects the performance of the radar detection at the Tx vehicle and the communication between the Tx and Rx vehicles. Consequently, we formulate the selection of ψ as an optimization problem in the next section.

4. Problem formulation

We define the optimum sub-carrier set size, denoted by ψ^* , as the one that maximizes the number of successfully transmitted bits/symbol between the Tx and Rx vehicles while keeping the target detection probability at the Tx vehicle above a specific threshold Δ . The problem is thus formulated as an integer optimization as follows

maximize
$$O(\psi) = P_{\text{SucDec}}(\psi) \times \log_2 \begin{pmatrix} \Psi \\ \psi \end{pmatrix}$$
, (14)

subject to
$$P_{\text{TarDet}}(\psi) \ge \Delta$$
, (15)

$$\psi \in \{1, 2, ..., \Psi\}. \tag{16}$$

The objective (14) is the number of successfully transmitted bits/symbol, which is the number of transmitted bits/symbol ($\log_2\binom{\Psi}{\psi}$) multiplied by the probability of successful symbol decoding (P_{SucDec}). Constraint (15) sets the minimum acceptable value (Δ) for target detection probability at the Tx vehicle (P_{TarDet}) while constraint (16) limits the size of the sub-carrier set to an integer value between 1 and Ψ . The probability of successful decoding, P_{SucDec} , and the target detection probability, P_{TarDet} , are the focus of the following two subsections, respectively.

4.1. Probability of successful decoding

When the Tx vehicle uses a sub-carrier set S_{ψ} (of size ψ) to represent some data symbol, the Rx vehicle can successfully decode that symbol when it correctly detects the presence of a signal

on S_{ψ} and no signal on the other $\Psi-\psi$ unused sub-carriers. Consequently, $P_{\rm SucDec}$ is evaluated as

$$P_{\text{SucDec}} = \prod_{k \in S_{\psi}} P_{D,k} \prod_{j \notin S_{\psi}} \left(1 - P_{FA,j} \right), \tag{17}$$

where $P_{D,k}$ and $P_{FA,k}$ are, respectively, the signal detection and false alarm probabilities on sub-carrier k. The Rx vehicle applies a simple binary hypothesis test independently on each sub-carrier to determine if the sub-carrier is used by the Tx vehicle. Since $P_{FA,k}$ is the probability that the magnitude of the received signal $r_{rx,k}$ exceeds a threshold V_{rx} when sub-carrier k is not used by the Tx vehicle (i.e., when $P_{tx,k} = 0$), thus

$$P_{FA,k} = P(r_{rx} \ge V_{rx,k} | P_{tx,k} = 0),$$
 (18a)

$$=\exp\left(-\frac{V_{rx}^2}{\sigma_n^2 + \sigma_{ry}^2}\right),\tag{18b}$$

where (18b) is by calculating (18a) for the Rayleigh PDF in (3). Similarly, $P_{D,k}$ is the probability that $r_{rx,k}$ exceeds the threshold V_{rx} but when sub-carrier k is actually used by the Tx vehicle (i.e., when $P_{rx,k} \neq 0$), hence

$$P_{D,k} = P(r_{rx,k} \ge V_{rx} | P_{tx,k} \ne 0).$$
 (19)

Calculating (19) using the PDFs in (9)), (10)) for the LoS/NLoS cases, $P_{D,k}$ becomes

$$P_{D,k} = \begin{cases} Q_1 \left(\sqrt{\frac{2s_{rx,k}^2}{\sigma_n^2 + \sigma_{rx}^2}}, \sqrt{\frac{2V_{rx}^2}{\sigma_n^2 + \sigma_{rx}^2}} \right), & \text{LoS}, \\ \exp\left(-\frac{V_{rx}^2}{s_{rx,k}^2 + \sigma_n^2 + \sigma_{rx}^2} \right), & \text{NLoS}, \end{cases}$$
(20)

where $Q_1\left(\cdot,\cdot\right)$ is the Marcum-Q function. The threshold V_{rx} is chosen to satisfy specific $P_{FA}^{\rm req}$ per sub-carrier in order not to overwhelm the Rx vehicle with false communication [15]. Hence, from (18b), the threshold is $V_{rx}=\sqrt{(\sigma_n^2+\sigma_{rx}^2)\log(1/P_{FA}^{\rm req})}$. Using the previously discussed assumptions of equal power allocation (i.e., $P_{tx,k}=P_{tx}/\psi$) and i.i.d. sub-carriers assumption, then $P_{\rm SucDec}$ becomes

$$P_{\text{SucDec}}(\psi) = \left(1 - P_{FA}^{\text{req}}\right)^{\Psi - \psi} \times \begin{cases} Q_1^{\psi} \left(\sqrt{\frac{2\Gamma_{rx}}{\psi}}, \sqrt{2\log\left(\frac{1}{P_{FA}^{\text{req}}}\right)}\right), & \text{LoS}, \\ \exp^{\psi} \left(-\frac{\log(1/P_{FA}^{\text{req}})}{1 + \Gamma_{rx}/\psi}\right), & \text{NLoS}, \end{cases}$$

where $\Gamma_{rx} = P_{tx} \gamma R^{-\alpha} / (\sigma_n^2 + \sigma_{rx}^2)$. By substituting with (21) in (14), we get a closed form expression for the number of successfully transmitted bits/symbol $O(\psi)$ as follows:

$$O(\psi) = \log_2 \left(\frac{\Psi}{\psi}\right) \left(1 - P_{FA}^{\text{req}}\right)^{\Psi - \psi} \times \begin{cases} Q_1^{\psi} \left(\sqrt{\frac{2\Gamma_{rx}}{\psi}}, \sqrt{2\log\left(\frac{1}{P_{FA}^{\text{req}}}\right)}\right), & \text{LoS}, \\ \exp^{\psi} \left(-\frac{\log(1/P_{FA}^{\text{req}})}{1 + \Gamma_{rx}/\psi}\right), & \text{NLoS}, \end{cases}$$
 (22)

4.2. Probability of target detection

The Tx vehicle determines the presence of a target (i.e., the Rx vehicle) if it can detect its reflected signal on any of its used sub-carriers (i.e., set S_{ψ}). Therefore, the probabilities of target detection/false alarm, respectively, are

$$P_{\text{TarDet}} = 1 - \prod_{k \in S_{w}} (1 - P_{TD,k}) \stackrel{a}{=} 1 - (1 - P_{TD,k})^{\psi},$$
 (23)

$$P_{\text{TarFA}} = 1 - \prod_{k \in S_{J_t}} (1 - P_{TFA,k}) \stackrel{a}{=} 1 - (1 - P_{TFA,k})^{\psi},$$
 (24)

where $P_{TD,k}$ and $P_{TFA,k}$ are the probabilities of detection and false alarm at the Tx vehicle on sub-carrier k. In both equations, $\stackrel{a}{=}$ follows from the assumption of i.i.d. channels and equal power allocation over the sub-carriers. Since $P_{TD,k}$ is the probability that $r_{tx,k}$ exceeds some threshold V_{tx} , i.e., $P_{TD,k} = P(r_{tx,k} \ge V_{tx})$ then using the PDFs in (12) and (13) for the LoS/NLoS cases, one gets

$$P_{TD,k} = \begin{cases} Q_1 \left(\sqrt{\frac{2S_{tx}^2}{\psi(\sigma_n^2 + \sigma_{tx}^2)}}, \sqrt{\frac{2V_{tx}^2}{\sigma_n^2 + \sigma_{tx}^2}} \right), & \text{LoS}, \\ 1 - \sqrt{\frac{V_{tx}^2}{S_{tx}^2/\psi + \sigma_{tx}^2}} G_{1,3}^{2,1} \left(\frac{V_{tx}^2}{S_{tx}^2/\psi + \sigma_{tx}^2} \right)_{0.5,0.5,-0.5}^{0.5}, & \text{NLoS}, \end{cases}$$

where $S_{tx}^2 = \Omega P_{tx} R^{-2\alpha} \gamma / 4\pi$. The expression of $P_{TD,k}$ in the NLoS case is obtained following the derivation of the Cumulative Distribution Function (CDF) of two multiplied independent Rayleigh RVs in [17].

If the Rx vehicle is not present, the magnitude of the signal received at the Tx vehicle follows a Rayleigh distribution such that P_{TEA} is

$$P_{TFA,k} = \exp\left(-\frac{V_{tx,k}^2}{\sigma_n^2 + \sigma_c^2 P_{tx}/\psi}\right),\tag{26}$$

where σ_c^2 is the variance of the radar signal reflected off clutter such as the vehicles in other lanes (per unit transmit power) and is given by

$$\sigma_c^2 = \frac{\Omega \gamma}{4\pi} \sum_{l} \mathbb{E}_{\Phi_l} \left[\sum_{i \in \Phi_l} d_i^{-2\alpha} \right]$$

$$\stackrel{a}{=} \frac{\Omega \gamma \zeta \tau}{2\pi} \sum_{l} \int_{x-ll/(2\pi)(\Theta/2)}^{\infty} \frac{dx}{((lL)^2 + x^2)^{\alpha}}.$$
(27)

Similar to (4), $\stackrel{a}{=}$ follows from the geometry of Fig. 1, the HPPP assumption, and Campbell's theorem [16]. The factor $\tau < 1$ is set to account for the fact that reflections from different vehicles arrive at different times (and therefore the summation is an over estimation of the clutter). It is worth noting that σ_c^2 has the following closed form at $\alpha = 2$

$$\sigma_c^2 = \frac{\Omega \gamma \zeta \tau}{4\Psi L^3} \left[\frac{\Theta}{2} - \frac{\tan{(\Theta/2)}}{\tan^2{(\Theta/2)} + 1} \right] \sum_l \frac{1}{l^3}.$$
 (28)

Finally, the detection threshold V_{tx} is chosen to satisfy a specific false alarm probability $P_{\text{TarFA}} = P_{FA}^{\text{req}}$ [15]. Hence, from (24) and (26), the value of the threshold is $V_{tx}(\psi) \approx \sqrt{(\sigma_n^2 + \sigma_c^2 P_{tx}/\psi) \log(\psi/P_{FA}^{\text{req}})}$, and the probability of target detection can now be written as

 $P_{\mathsf{TarDet}}(\psi)$

$$= \begin{cases} 1 - \left(1 - Q_1 \left(\sqrt{\frac{2S_{tx}^2}{\psi(\sigma_n^2 + \sigma_{tx}^2)}}, \sqrt{\frac{2V_{tx}^2(\psi)}{\sigma_n^2 + \sigma_{tx}^2}}\right)\right)^{\psi}, & \text{LoS}, \\ 1 - \left(\sqrt{\frac{V_{tx}^2(\psi)}{S_{tx}^2/\psi + \sigma_{tx}^2}}G_{1,3}^2 \left(\frac{V_{tx}^2(\psi)}{S_{tx}^2/\psi + \sigma_{tx}^2}\right|_{0.5, 0.5, -0.5}^{0.5}\right)\right)^{\psi}, & \text{NLoS} \end{cases}$$

$$(29)$$

5. Proposed optimization algorithms

The analysis in the previous section shows that the selection of ψ (for LoS and NLoS) is a non-linear integer optimization problem with a non-concave constraint and non-concave and non-differentiable objective, and consequently is hard to solve. Fortunately, the problem has a single optimization variable ψ over a finite integer set, which makes search algorithms feasible. We use in Section 5.1 a Segmented Hill Climbing (SHC) algorithm to find the optimum solution for the exact LoS/NLoS problems. We also show in Section 5.2 that a real concave relaxed version of the NLoS problem can be solved using the Karush Kuhen Tucker (KKT) conditions and a one-off branching.

5.1. Segmented hill climbing solution

Hill climbing is a local search algorithm that starts at some point and moves the search in the direction of objective increase [18]. The constraint is handled using a rejection strategy where solutions that violate the constraint are rejected during the search [19]. To this end, we add the constraint to the objective in the form of a boolean function such that the new objective is

$$\tilde{O}(\psi) = O(\psi) \times 1(P_{\text{TarDet}}(\psi) \ge \Delta), \tag{30}$$

where $1(u \ge Z)$ is 1 if $u \ge Z$ and 0 otherwise. We detail the steps of the proposed SHC solution in Algorithm 1.

Algorithm 1 Segmented Hill climbing (SHC).

```
1: Divide the set \{1, 2, ..., \Psi\} to I non-overlapping segments.
 2: For i = 1:I
        Define the start and end points of segment i(\psi_{st}, \psi_{end})
 3.
         If \psi_{st} feasible & \psi_{end} infeasible
           Set initial search point \psi = \psi_{si}
         ElseIf \psi_{st} infeasible & \psi_{end} feasible
           Set initial search point \psi = \psi_{end}
  7:
 8:
         Elself \psi_{st} infeasible & \psi_{end} infeasible
 9:
           Skip segment i
10:
           Set initial search point \psi randomly between \psi_{st} and \psi_{end}
11:
12:
         End If
         If \psi + 1 \le \psi_{end} \& \tilde{O}(\psi + 1) \ge \tilde{O}(\psi)
13:
14:
15:
         ElseIf \psi - 1 \ge \psi_{st} \& \tilde{O}(\psi - 1) \ge \tilde{O}(\psi)
16:
17
18:
19:
         Else
20:
           Skip segment i
21:
         End If
22.
         While (1)
         If Dir == 1 \& \psi + 1 \le \psi_{end} \& \tilde{O}(\psi + 1) \ge \tilde{O}(\psi)
23:
25:
         Elself Dir == -1 \& \psi - 1 \ge \psi_{st} \& \tilde{O}(\psi - 1) \ge \tilde{O}(\psi)
26:
27:
28:
           Dir = -1
         Else
         End If
         End While
         \tilde{\psi}[i] = \psi, \ O^* = \tilde{O}(\tilde{\psi})
         If \psi_{end} \geq \Psi/2 & !isempty(\tilde{\psi})
           Break
         End If
37: End For
38: \psi^* = \tilde{\psi}(\operatorname{argmax}(O^*))
```

The search domain is first divided into equal sized non-overlapping segments (step 1). The segmentation helps skip infeasible segments (steps 9 and 20) and terminate the search early when the optimal solution is found (step 30). In each segment, the algorithm defines its initial search point based on the feasibility of the segments end points (steps 3-12). The algorithm then searches

in the direction of objective increase, updates the search point in that direction, and saves this direction (steps 13-21). The algorithm keeps moving in the saved direction till no improvement happens or the solution becomes infeasible (steps 22-32). After that, the optimum solution is obtained by comparing the optimum solutions of the different segments (step 38). A closer inspection of the unconstrained objective in (14) shows that $\psi^* \leq \Psi/2$ (since $\begin{pmatrix} \Psi \\ \psi \end{pmatrix}$ decreases after $\Psi/2$ and P_{SucDec} decreases with ψ . This observation allows the early termination of the algorithm if an optimal feasible solution is found in the range $\{1,2,...\Psi/2\}$ (steps 34-36). It is important to notice that in the limit that segment size is 1 and no early stopping criterion, the SHC behaves like an exhaustive search algorithm that checks every point in the optimization domain $\{1,2,...,\Psi\}$.

The complexity of SHC is $\mathcal{O}_1 + \mathcal{O}_2$ where \mathcal{O}_1 is the complexity of steps 2-37 in Algorithm 1 and \mathcal{O}_2 is the complexity of step 38. \mathcal{O}_1 is $\mathcal{O}\left(\sum_{i=1}^I N_i\right)$ where I is the number of segments and $1 \leq N_i \leq \Psi/I$ is the number of searched points in segment i. Consequently, $\mathcal{O}(I) \leq \mathcal{O}_1 \leq \mathcal{O}(\Psi)$. Assuming that N_i has uniform distribution over its range, then \mathcal{O}_1 has an average complexity of $\mathcal{O}\left(0.5I(\Psi/I+1)\right) \approx \mathcal{O}\left(\Psi\right)$. Also, \mathcal{O}_2 is the complexity of sorting an array of I elements. We assume, for simplicity, a selection sort with complexity $\mathcal{O}\left(I^2\right)$ (other sorting algorithms have lower complexities) Combining \mathcal{O}_1 and \mathcal{O}_2 shows that SHC has equal average and worst complexities of $\mathcal{O}\left(\Psi+I^2\right)$ and best case complexity of $\mathcal{O}\left(I+I^2\right) \approx \mathcal{O}\left(I^2\right)$.

5.2. Real concave relaxation for the NLoS case

This section relaxes the NLoS problem to become a real concave optimization problem that can be solved by the KKT conditions. The NLoS objective is relaxed by taking its logarithm and using the approximation $\log(n!) \approx n \log n - n \log e$ as follows

$$\log O(\psi) \approx (\Psi - \psi) \log(1 - P_{FA}^{\text{req}}) - \frac{\psi^2 \log(1/P_{FA}^{\text{req}})}{\psi + \Gamma_{rx}}$$
$$- \log(\log(2)) + \log(\Psi \log(\Psi) - \psi \log(\psi)$$
$$- (\Psi - \psi) \log(\Psi - \psi). \tag{31}$$

The approximate log objective is concave as it is the sum of a linear term, a concave term, and the log of a concave function, which is concave too, from function composition [20]. To simplify P_{TarDet} in the NLoS case, we ignore the channel effect on the reflected signal from the Rx vehicle to the Tx vehicle. In this case, the magnitude of the received reflected signal at the Tx vehicle has a Rayleigh PDF and consequently, the probability of target detection is

$$P_{\text{TarDet}}(\psi) \approx 1 - \left(1 - \exp\left(-\frac{(\sigma_n^2 \psi + \sigma_c^2) \log(\psi/P_{FA}^{\text{req}})}{S_{tx}^2 + \psi(\sigma_n^2 + \sigma_{tx}^2)}\right)\right)^{\psi}.$$
(32)

The constraint $P_{\text{TarDet}} \ge \Delta$ can hence be reformulated as

$$g(\psi) = \psi \log (1 - \exp(-f(\psi))) \le \log(1 - \Delta),$$
 (33)

where
$$f(\psi) = \frac{\psi \sigma_n^2 + \sigma_c^2}{\psi (\sigma_n^2 + \sigma_{tx}^2) + S_{tx}^2} \log(\Psi/P_{FA}^{\text{req}}), \tag{34}$$

where we substituted with Ψ instead of ψ inside the log in $f(\psi)$, which is an over estimation of the detection threshold to further simplify the constraint. In what follows, we show that the simplified constraint in (33) is quasi-convex when $\sigma_n^2 \approx 0$ (when

the clutter dominates the noise), which is considered to be the dominant case in vehicular systems where signal reflections and interference dominate the noise. We start with the derivative of $g(\psi)$ given by

$$\nabla g(\psi) = \log(1 - \exp(-f(\psi))) + \frac{\psi \nabla f(\psi)}{\exp(f(\psi)) - 1}, \quad (35)$$

where
$$\nabla f(\psi) = \frac{\sigma_n^2 S_{tx}^2 - \sigma_c^2 (\sigma_n^2 + \sigma_{tx}^2)}{(\psi(\sigma_n^2 + \sigma_{tx}^2) + S_{tx}^2)^2}.$$
 (36)

From the equation above, if $\sigma_n^2 \approx 0$, $\nabla f(\psi)$ (and consequently $\nabla g(\psi)$) is negative over all ψ . This means that $g(\psi_2) < g(\psi_1) < g(\psi_0)$ for any $\psi_0 < \psi_1 < \psi_2$ and consequently, the quasi-convexity condition $g(\psi_1) < \max(g(\psi_0), g(\psi_2))$ is always satisfied.

Based on the above discussion, the log objective in (31) is concave and the simplified constraint in (33) is quasi-convex, hence a point ψ^* satisfying the KKT conditions is a global maximum [21]. The KKT conditions are given by [20]

$$\nabla \log O(\psi^*) + \lambda^* \nabla g(\psi^*) = 0, \tag{37}$$

$$\lambda^* > 0, \tag{38}$$

$$\lambda^* g(\psi^*) = 0, \tag{39}$$

where λ^* is the optimal dual (Lagrange) price. Substituting with (37) in (39), then $\lambda^* = -\nabla \log O(\psi^*)/\nabla g(\psi)$ and $-g(\psi^*)\nabla \times \log O(\psi^*)/\nabla g(\psi^*) = 0$. Since $\nabla \log O(\psi)$ is the first derivative of the log objective w.r.t. ψ , it is given by

 $\nabla \log O(\psi)$

$$= -\log\left((1 - P_{FA}^{\text{req}})\right) - \log\left(\frac{1}{P_{FA}^{\text{req}}}\right) \left(1 - \frac{\Gamma_{rx}^{2}}{(\Gamma_{rx} + \psi)^{2}}\right)$$
$$-\frac{\log\left(\frac{\psi}{\Psi - \psi}\right)}{\Psi \log(\Psi) - \psi \log(\psi) - (\Psi - \psi) \log(\Psi - \psi)}.$$
 (40)

The solution of the KKT conditions is summarized in Algorithm 2. The solution ψ^* is usually real (non-integer), and consequently to get an integer solution we use one-off branching where we consider the two solutions $\lfloor \psi^* \rfloor$ and $\lceil \psi^* \rceil$ and choose the feasible one with higher objective.

Algorithm 2 Solving the KKT conditions.

```
1: Assume a trivial solution with \lambda^* = 0 and solve \nabla \log O(\tilde{\psi}) = 0 for \tilde{\psi}
2: If g(\tilde{\psi}) \leq \log(1 - \Delta)
3: \psi^* = \tilde{\psi} and \lambda^* = 0
4: Else
5: Find the other roots of g(\psi)\nabla \log O(\psi) = 0
6: If any root \tilde{\psi} has -\nabla \log O(\tilde{\psi})/\nabla g(\tilde{\psi}) > 0
7: \psi^* = \tilde{\psi} and \lambda^* = -\nabla \log O(\psi)/\nabla g(\tilde{\psi})
8: Else
9: The problem is infeasible
10: End If
11: End If
```

6. RSS-based estimation of inter-vehicle distance at Rx vehicle

As shown in the previous sections, the Rx vehicle detects the signal received on different sub-carriers in order to decode the information message. In this section, we propose that the Rx vehicle also uses the RSS on different sub-carriers to estimate R between the Tx vehicle and itself. In this case, the estimation of R at Rx and the communication between Tx and Rx are two byproducts of the radar signal of the Tx vehicle. To this end, we derive the

Maximum Likelihood based Estimation (MLE), which is the estimate that maximizes the log-likelihood function (LL) of the magnitude of the received signal over the used sub-carriers such that

$$LL = \sum_{k=1}^{\psi} \log (f_{r_{rx,k}}(r))$$
 in the two following cases [22].

6.1. NLoS between Tx and Rx vehicles

From the PDF of $r_{rx,k}$ in (10), the LL function is

$$LL_{NLOS} = \sum_{k=1}^{\psi} \log(2r_k) - \psi \log(\sigma_{rx}^2 + \sigma_n^2 + au) - \frac{\sum_{k=1}^{\psi} r_k^2}{\sigma_{rx}^2 + \sigma_n^2 + au}$$
(41)

where $a=P_{tx}\gamma/\psi$ and $u=R^{-\alpha}$. Solving $\partial LL_{NLoS}/\partial u=0$ gives the MLE \hat{u}_{ML} as follows

$$\hat{u}_{ML} = \frac{\psi}{P_{tx}\gamma} \left[\frac{1}{\psi} \sum_{k=1}^{\psi} r_{rx,k}^2 - \sigma_{rx}^2 - \sigma_n^2 \right]. \tag{42}$$

From the form of (42), it can be deduced that \hat{u}_{ML} is an efficient unbiased estimator [22], which has a Mean Squared Error (MSE) that coincides with the Cramer-Rao bound (CRB) defined as

$$CRB = \left(\psi \mathbb{E}_r \left[\left(\frac{\partial \log(f(r))}{\partial u} \right)^2 \right] \right)^{-1}. \tag{43}$$

Clearly, since $\log(f(r)) = \log(2r) - \log(\sigma_{r\chi}^2 + \sigma_n^2 + au) - \frac{r^2}{\sigma_{r\chi}^2 + \sigma_n^2 + au}$, hence

$$\frac{\partial \log(f(r))}{\partial u} = \frac{-a}{\sigma_{rx}^2 + \sigma_r^2 + au} \left[1 - \frac{r^2}{\sigma_{rx}^2 + \sigma_r^2 + au} \right],\tag{44}$$

and

$$\mathbb{E}_{r} \left[\left(\frac{\partial \log(f(r))}{\partial u} \right)^{2} \right]$$

$$= \left(\frac{a}{\sigma_{rx}^{2} + \sigma_{n}^{2} + au} \right)^{2}$$

$$\times \left[1 - \frac{2\mathbb{E}_{r} \left[r^{2} \right]}{\sigma_{rx}^{2} + \sigma_{n}^{2} + au} + \frac{\mathbb{E}_{r} \left[r^{4} \right]}{\left(\sigma_{rx}^{2} + \sigma_{n}^{2} + au \right)^{2}} \right],$$

$$= \left(\frac{a}{\sigma_{rx}^{2} + \sigma_{n}^{2} + au} \right)^{2}, \tag{45}$$

and one can conclude that

$$CRB_{NLoS} = \frac{1}{\psi} \left(R^{-\alpha} + \frac{\psi \left(\sigma_{rx}^2 + \sigma_n^2 \right)}{P_{tx} \gamma} \right)^2. \tag{46}$$

6.2. LoS between Tx and Rx vehicles

We follow the analysis in the previous subsection for the LoS case. From (9), the log-likelihood function is

$$LL_{LoS} = \sum_{k=1}^{\psi} \log \left(\frac{2r_k}{\sigma_{rx}^2 + \sigma_n^2} \right) - \sum_{k=1}^{\psi} \frac{r_k^2 + P_{tx} \gamma R^{-\alpha} / \psi}{\sigma_{rx}^2 + \sigma_n^2} + \sum_{k=1}^{\psi} \log \left(I_0 \left(\frac{2r_k P_{tx} \gamma R^{-\alpha} / \psi}{\sigma_{rx}^2 + \sigma_n^2} \right) \right).$$
(47)

Table 1Simulation parameters.

*	
Radar cross section, Ω	30 dB s m
Radar antenna power gain, G	45 dB
Radar transmission power, P_{tx}	10 dB m
Radar antenna beamwidth, Θ	15°
Effective antenna aperture, A_e	0.0387
Pathloss exponent, α	2
Noise power, σ_n^2 ,	10^{-14}
Tx-Rx distance, R,	20 m
Total number of sub-carriers, Ψ ,	16
Lane width, L	4 m
Number of lanes in the road	3
Density of interfering vehicle per lane, ζ	$5~\mathrm{km}^{-1}$
False alarm probability, P_{FA}^{req}	10^{-4}
Minimum target detection probability, Δ	0.9

For mathematical tractability, we use a Gaussian approximation of the Ricean PDF in (9) such that $r_{rx,k} \sim \mathcal{N}(\sqrt{P_{tx}\gamma\,R^{-\alpha}/\psi},(\sigma_{rx}^2+\sigma_n^2)/2)$. This approximation is valid at high Signal to Interference plus Noise Ratio (SINR) when the power of the desired signal at the Rx vehicle is stronger than the interference and noise signals (i.e., $P_{tx}\gamma\,R^{-\alpha}/\psi >> \sigma_{rx}^2+\sigma_n^2$))). Using the simplified distribution, the log-likelihood function can be written as follows

$$LL_{LoS} \approx -\psi \log \left(\sqrt{\pi \left(\sigma_{rx}^2 + \sigma_n^2\right)} - \sum_{k=1}^{\psi} \frac{(r_k - b\nu)^2}{\sigma_{rx}^2 + \sigma_n^2},$$
 (48)

where $v=R^{-\alpha/2}$ and $b=\sqrt{P_{tx}\gamma/\psi}$. Solving $\partial LL_{LoS}/\partial v=0$ gives the MLE \hat{v}_{ML} as follows

$$\hat{v}_{ML} = \sqrt{\frac{1}{P_{tx}\gamma\psi}} \sum_{k=1}^{\psi} r_{rx,k}.$$
(49)

From the form of (49), it can be observed that the MLE is an efficient unbiased estimator with its MSE coinciding with the CRB, which is obtained using the same definition in (43) after replacing u with v in the following steps:

$$\log(f(r)) = -\log(\sqrt{\pi(\sigma_n^2 + \sigma_{rx}^2)}) - \frac{(r - bv)^2}{(\sigma_r^2 + \sigma_r^2)},$$
 (50)

$$\frac{\partial \log(f(r))}{\partial v} = \frac{2b}{\sigma_n^2 + \sigma_{rx}^2} (r - bv),\tag{51}$$

nd

$$\mathbb{E}_{r}\left[\left(\frac{\partial \log(f(r))}{\partial v}\right)^{2}\right] = \frac{4b^{2}\left[b^{2}v^{2} - 2bv\mathbb{E}_{r}[r] + \mathbb{E}_{r}[r^{2}]\right]}{(\sigma_{n}^{2} + \sigma_{rx}^{2})^{2}}$$

$$= \frac{2b^{2}}{\sigma_{n}^{2} + \sigma_{rx}^{2}}.$$
(52)

And, consequently,

$$CRB_{LOS} = \frac{(\sigma_n^2 + \sigma_{rx}^2)}{2P_{tx}\gamma}.$$
 (53)

7. Numerical results

This section presents the numerical results of the LoS/NLoS cases. For simulations, we use Monte-Carlo Matlab simulation. The figures are generated using the parameters in Table 1 [14] unless stated otherwise

We start with Fig. 4, which sketches the number of successfully transmitted bits/symbol $O(\psi)$ (on the left vertical axis) and the target detection probability $P_{\text{TarDet}}(\psi)$ (on the right vertical

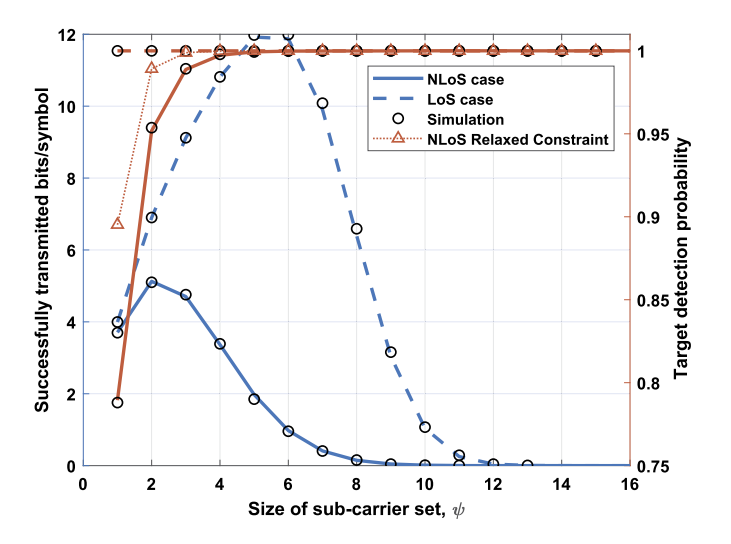
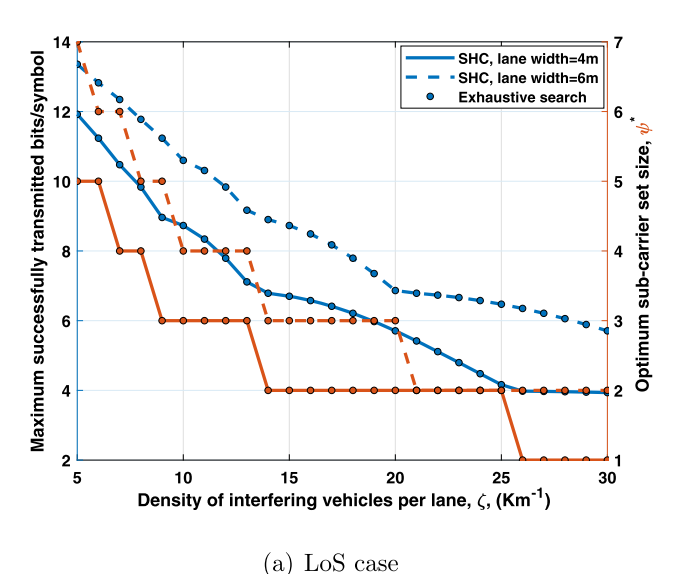


Fig. 4. Successfully transmitted bits/symbol and target detection probability versus the size of sub-carriers set in the LoS/NLoS cases.



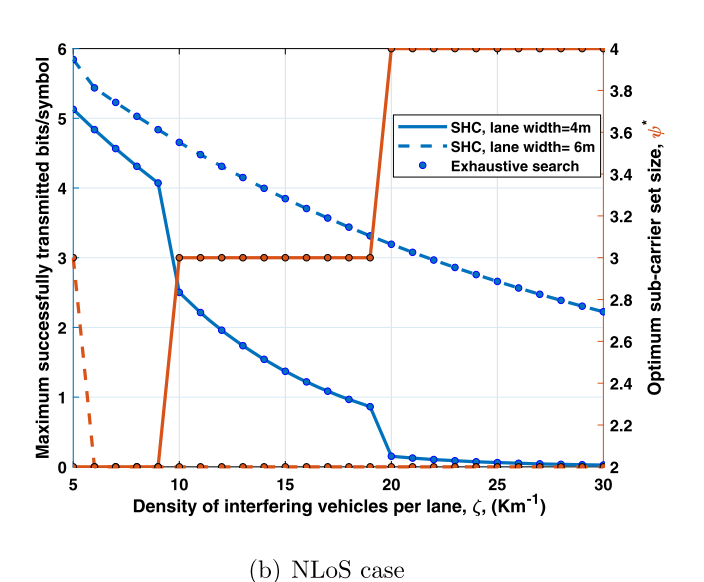
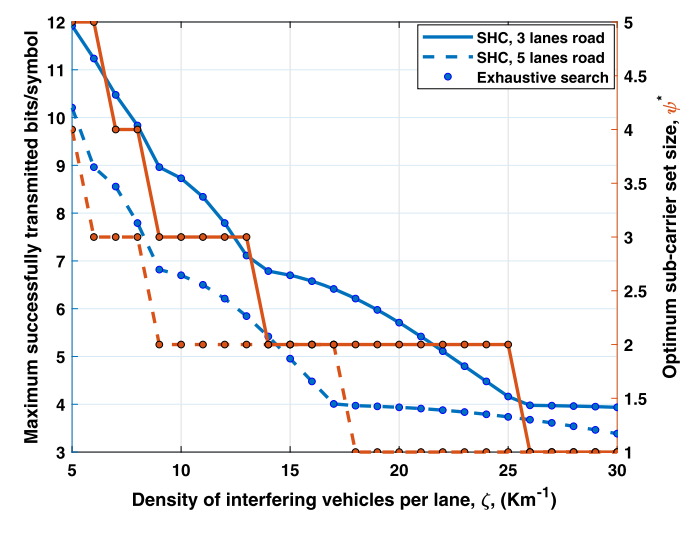


Fig. 5. The maximum number of successfully transmitted bits/symbol and the optimum sub-carrier set size versus the density of interfering vehicles per lane (for different lane widths).



(a) LoS case

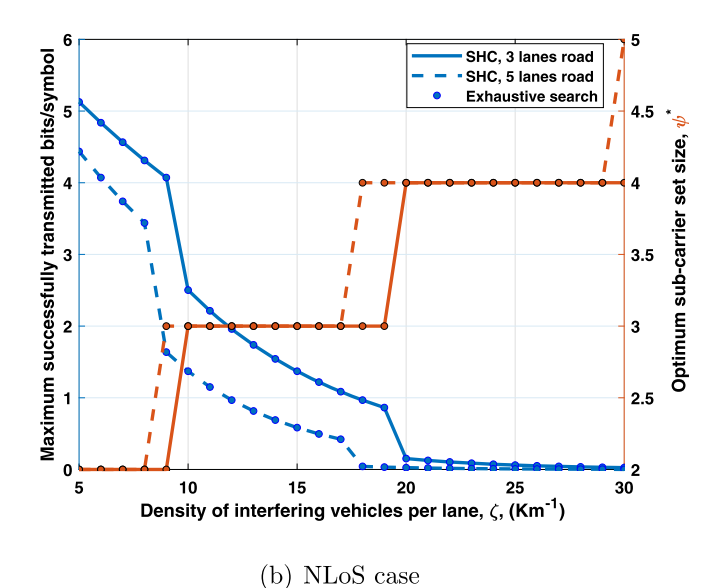


Fig. 6. The maximum number of successfully transmitted bits/symbol and the optimum sub-carrier set size versus the density of interfering vehicles per lane (for different number of lanes on road).

axis) versus the size of the sub-carrier set ψ (on the horizontal axis). The figure verifies the accuracy of the theoretical analysis of the LoS/NLoS cases by comparing the simulation results with the formulas derived in (22) and (29). As expected, $O(\psi)$ peaks at some optimum ψ^* ; the value of $O(\psi)$ decreases at $\psi < \psi^*$ due to under-utilized modulation (i.e., small constellation size) and also at $\psi > \psi^*$ due to reduced successful decoding probability $P_{\text{SucDec}}(\psi)$. As seen from the figure, the presence of LoS allows the successful transmission of more bits/symbol this is because the presence of LoS between the Tx-Rx improves P_{SucDec} , and consequently, a bigger constellation size can be used. The figure also shows that the LoS improves P_{TarDet} and that the relaxed NLoS P_{TarDet} in (32) is an over estimation of the NLoS P_{TarDet} in (29) because it ignored the channel effect on the reflected signal strength. However, the relaxed problem can be solved directly using the KKT constraints, and consequently it can operate as an upper bound to the system performance in the NLoS case.

Figs. 5, 6, and 7 show the optimum size of the sub-carrier set, ψ^* , and the maximum number of successfully transmitted

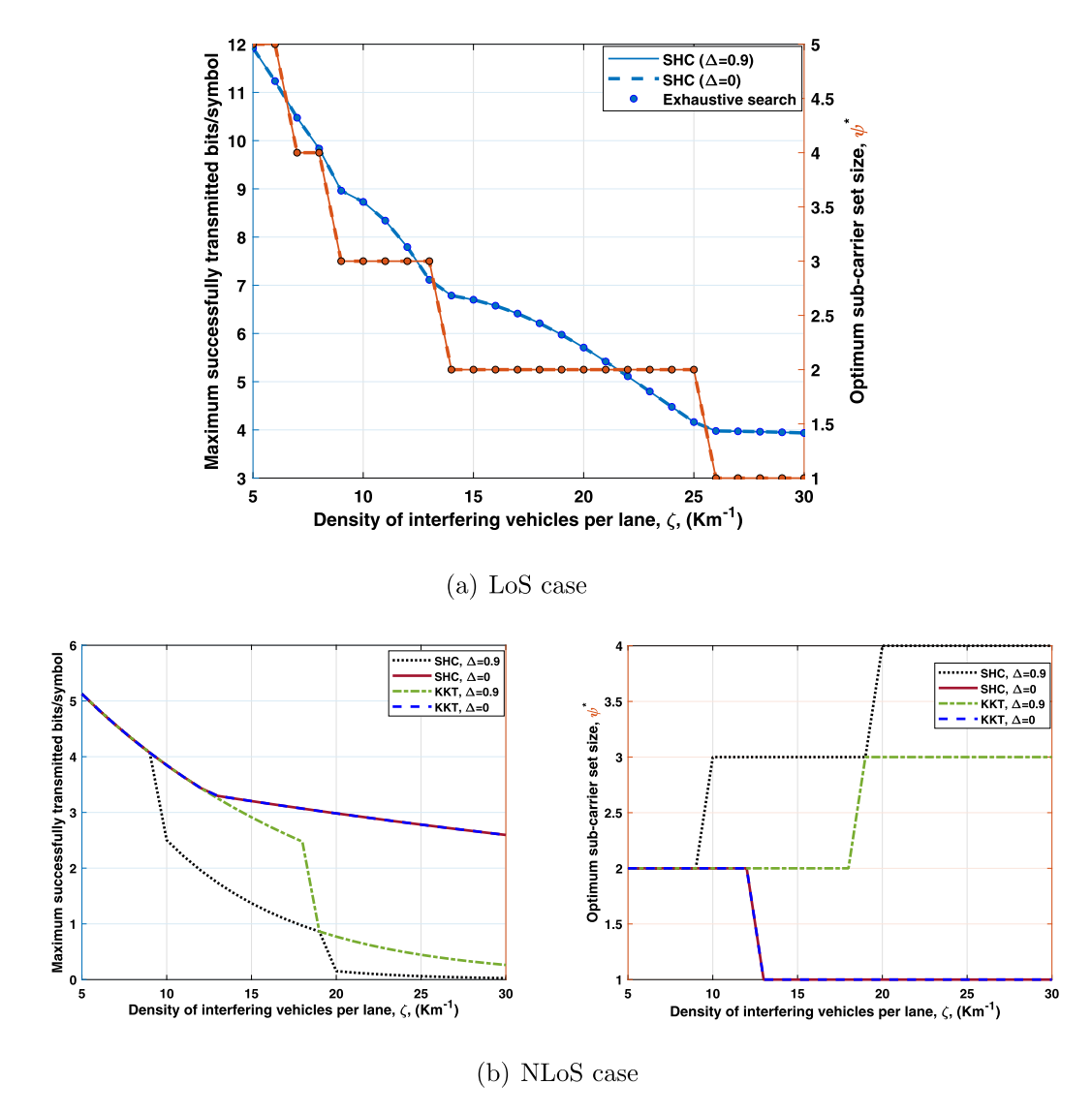
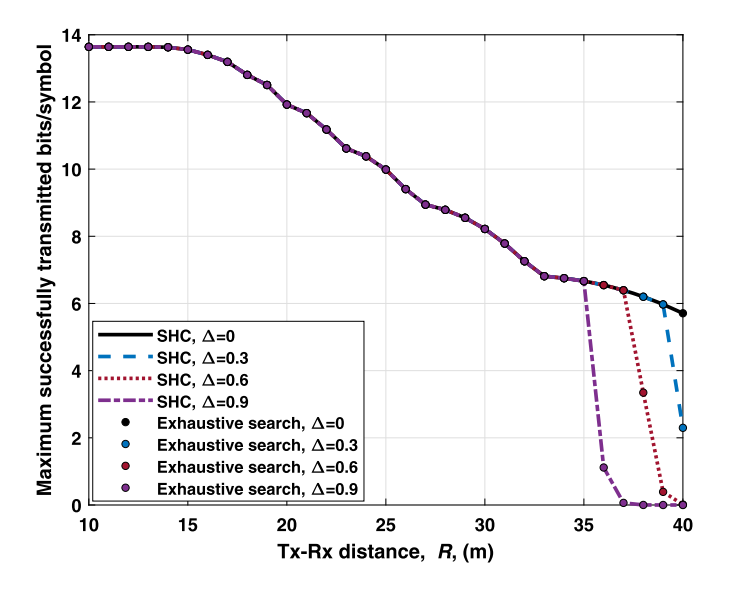


Fig. 7. The maximum number of successfully transmitted bits/symbol and the optimum sub-carrier set size versus the density of interfering vehicles per lane (for different P_{TarDet} requirement).

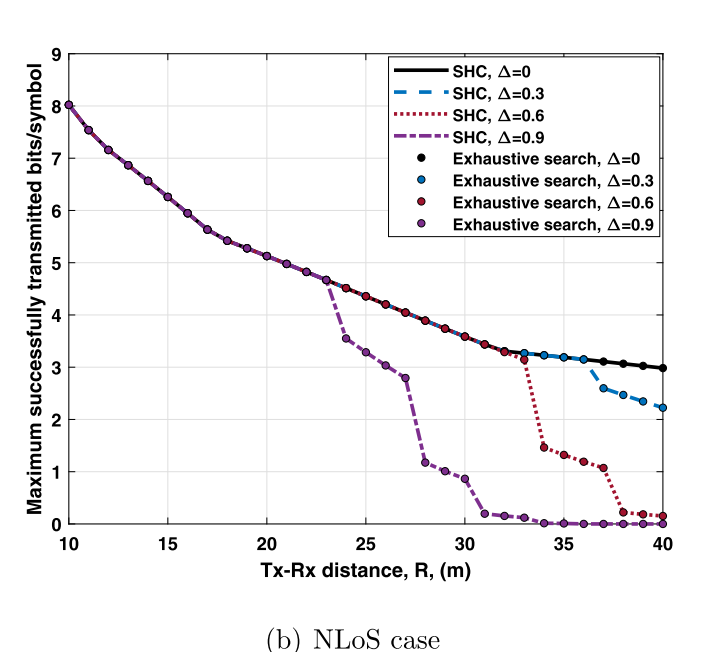
bits/symbol, $O(\psi^*)$, versus the density of interfering vehicles per lane, ζ , in both LoS and NLoS cases. The values of ψ^* and $O(\psi^*)$ are obtained by solving the optimization problem defined in (14), (15), and (16). The figures consider different conditions; specifically, Fig. 5 considers different lane widths, L, Fig. 6 considers roads with different number of lanes, while Fig. 7 considers different requirements of the target detection probability, Δ . The figures show that $O(\psi^*)$ decreases with increasing ζ due to the increased interference, which lowers the successful decoding probability and consequently lowers the maximum number of successfully transmitted bits/symbol. It is generally observed from the figures that more bits/symbol can be successfully transmitted in case of LoS between the Tx and Rx vehicles due to improved channel condition. Another observation is that in most NLoS cases, increasing ζ increases ψ^* in order to satisfy the constraint on P_{TarDet} (as higher ψ represents higher diversity for target detection). On the other hand, in LoS cases when P_{TarDet} is already higher than the required value (i.e., the constraint on P_{TarDet} is already satisfied), then increasing ζ decreases ψ^* in order to improve P_{SucDec} . As seen, wider lanes (in Fig. 5) and/or fewer interfering lanes (in Fig. 6) allow successful transmission of more bits/symbols due to reduced interference from neighbor lanes. Moreover, Fig. 7 shows the effect of the constraint $P_{\text{TarDet}} \geq \Delta$ on ψ^* and $O(\psi^*)$. As seen,

increasing Δ requires the use of more sub-carriers (i.e., higher ψ^*) in the NLoS case to satisfy the constraint, and consequently, $O(\psi^*)$ decreases as ψ^* shifts from the optimum value calculated at $\Delta = 0$ (i.e., when the problem is unconstrained). The figure also shows that the SHC solution of the exact NLoS problem and the KKT solution of the relaxed NLoS problem are the same when $\Delta = 0$ (i.e., when the problem is unconstrained). However, when $\Delta = 0.9$, the maximum successfully transmitted bits/symbol obtained from the KKT solution of the relaxed NLoS problem is an over estimation of the actual maximum successfully transmitted bits/symbol obtained from the solution of the exact NLoS problem. This is because the relaxed NLoS P_{TarDet} in (32) is an over estimation of the actual NLoS P_{TarDet} in (29) as evident from Fig. 4. On the other hand, increasing Δ does not affect the results in the LoS case because the value of ψ^* that maximizes the number of successfully transmitted bits/symbol of the unconstrained problem (i.e., when $\Delta = 0$) already yields high P_{TarDet} due to the better channel condition between the transmit and receive vehicles (compared to the NLoS case).

Fig. 8 shows the maximum number of successfully transmitted bits/symbol between the Tx and Rx vehicles versus their inter-distance. A longer distance means reduced received signal strengths and therefore lower bits/symbol. The number of



(a) LoS case



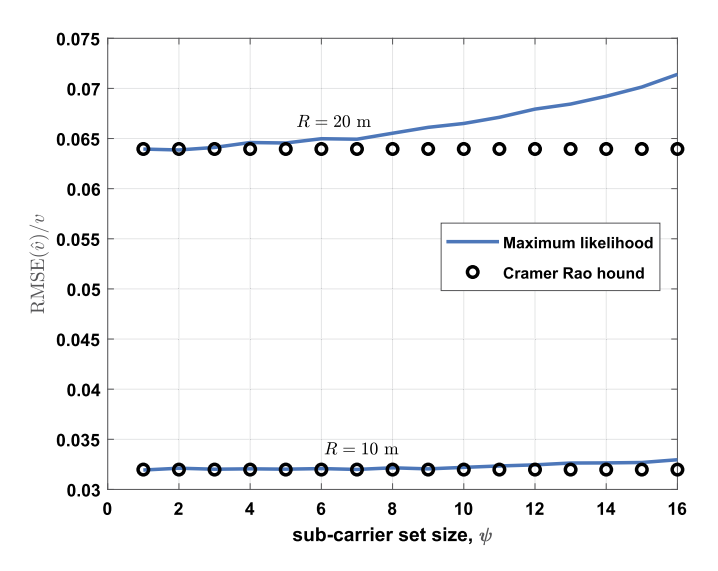
(b) Tibos case

 $\label{eq:Fig.8.} \textbf{Fig. 8.} \ \ \text{The maximum number of successfully transmitted bits/symbol vs the Tx-Rx distance.}$

bits/symbol is further reduced when tightening the constraint on P_{TarDet} as the transmitter shifts from the optimum constellation size in order to increase P_{TarDet} .

As shown in Figs. 5–8, SHC has the same performance as exhaustive search, but with much fewer iterations. The average number of iterations of SHC is found to be 5 with a standard deviation of 2 iterations compared to 16 iterations in case of exhaustive search.

Finally, Fig. 9 shows the normalized RMSE of the MLE versus the sub-carrier set size ψ for the LoS/NLoS cases. As shown in the figure, the MLE achieves the CRB in the NLoS case while in the LoS case, as explained in the analysis in Section 6.2, the Gaussian approximation of the received signal becomes more accurate at higher SINR. Therefore, the RMSE of the Gaussian MLE approaches the CRB when the Tx vehicle is close to the Rx vehicle and also when the Tx vehicle distributes its transmission



(a) LoS case

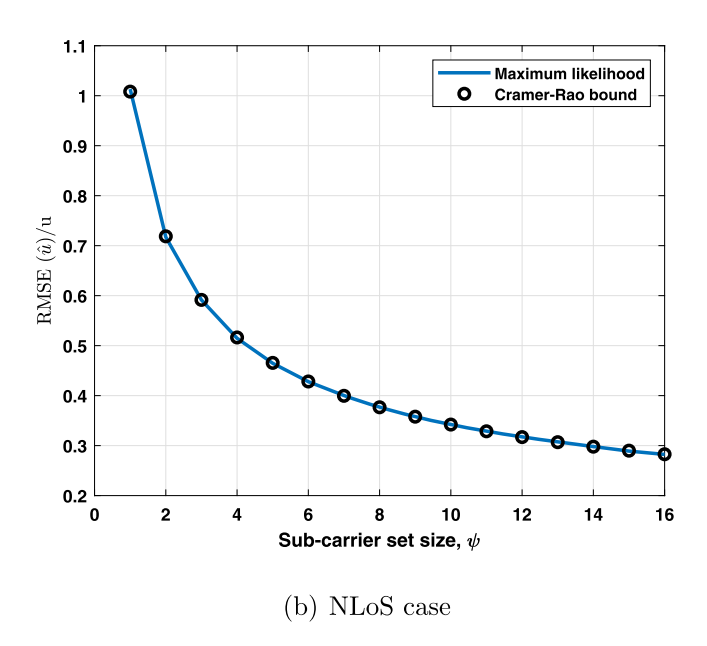


Fig. 9. The normalized RMSE of the maximum likelihood compared with the normalized squared root of the CRB versus ψ .

power over fewer sub-carriers (i.e., small $\psi\,)$ as evident from the figure.

8. Conclusion

This paper proposes an optimization framework for dual function radar and communication in vehicular systems. The framework maximizes the number of successfully transmitted bits between two vehicles subject to constraints on the radar performance for different road, traffic, and channel conditions. Results show that rates up to 12 (5) bits/symbol are possible for distances up to 20 m in LoS (NLoS) cases. The paper also suggested that the receive vehicle uses the received signal strength of the transmit vehicle not only to decode the embedded information, but to estimate the inter-vehicle distance as well. The analysis presented in this paper can be extended to include errors in range and velocity estimation as well as inter-carrier interference, and to integrate different techniques for mitigating inter-vehicle interference.

Declaration of competing interest

Mahmoud H. Ismail reports financial support was provided by American University of Sharjah. Ahmed S. Ibrahim reports financial support was provided by National Science Foundation.

References

- [1] M.Z. Chowdhury, M.T. Hossan, A. Islam, Y.M. Jang, A comparative survey of optical wireless technologies: architectures and applications, IEEE Access 6 (2018) 9819–9840
- [2] O.B. Akan, M. Arik, Internet of radars: sensing versus sending with joint radarcommunications, IEEE Commun. Mag. 58 (9) (2020) 13–19.
- [3] A. Hassanien, M.G. Amin, E. Aboutanios, B. Himed, Dual-function radar communication systems: a solution to the spectrum congestion problem, IEEE Signal Process. Mag. 36 (5) (2019) 115–126.
- [4] C. Wang, J. Tong, G. Cui, X. Zhao, W. Wang, Robust interference cancellation for vehicular communication and radar coexistence, IEEE Commun. Lett. 24 (10) (2020) 2367–2370.
- [5] C. Aydogdu, M.F. Keskin, N. Garcia, H. Wymeersch, D.W. Bliss, Radchat: spectrum sharing for automotive radar interference mitigation, IEEE Trans. Intell. Transp. Syst. 22 (1) (2021) 416–429.
- [6] D. Ma, T. Huang, Y. Liu, X. Wang, A novel joint radar and communication system based on randomized partition of antenna array, in: IEEE International Conference on Acoustics, Speech and Signal Processing, ICASSP, 2018, pp. 3335–3339.
- [7] E. Basar, M. Wen, R. Mesleh, M. Di Renzo, Y. Xiao, H. Haas, Index modulation techniques for next-generation wireless networks, IEEE Access 5 (2017) 16693–16746.
- [8] S.D. Tusha, A. Tusha, E. Basar, H. Arslan, Multidimensional index modulation for 5G and beyond wireless networks, Proc. IEEE 109 (2) (2020) 170–199.
- [9] S. Sugiura, T. Ishihara, M. Nakao, State-of-the-art design of index modulation in the space, time, and frequency domains: benefits and fundamental limitations, IEEE Access 5 (2017) 21774–21790.

- [10] T. Mao, Q. Wang, Z. Wang, S. Chen, Novel index modulation techniques: a survey, IEEE Commun. Surv. Tutor. 21 (1) (2018) 315–348.
- [11] E. BouDaher, A. Hassanien, E. Aboutanios, M.G. Amin, Towards a dual-function MIMO radar-communication system, in: IEEE Radar Conference, RadarConf, 2016, pp. 1–6.
- [12] X. Wang, A. Hassanien, M.G. Amin, Dual-function MIMO radar communications system design via sparse array optimization, IEEE Trans. Aerosp. Electron. Syst. 55 (3) (2018) 1213–1226.
- [13] X. Wang, J. Xu, Co-design of joint radar and communications systems utilizing frequency hopping code diversity, in: IEEE Radar Conference, RadarConf, 2019, pp. 1–6.
- [14] A. Al-Hourani, R.J. Evans, S. Kandeepan, B. Moran, H. Eltom, Stochastic geometry methods for modeling automotive radar interference, IEEE Trans. Intell. Transp. Syst. 19 (2) (2017) 333–344.
- [15] M. Richards, J. Scheer, W. Holm, W. Melvin, Principles of Modern Radar: Basic Principles, SciTech Publishing, New Jersey, 2010.
- [16] J. Andrews, A. Gupta, H. Dhillon, A primer on cellular network analysis using stochastic geometry, preprint, arXiv:1604.03183, 2016.
- [17] J. Salo, H.M. El-Sallabi, P. Vainikainen, The distribution of the product of independent Rayleigh random variables, IEEE Trans. Antennas Propag. 54 (2) (2006) 639–643
- [18] A. Jamal, Global optimization using local search approach for course scheduling problem, in: Scheduling Problem-New Applications and Trends, IntechOpen, 2019.
- [19] E.-G. Talbi, Metaheuristics: From Design to Implementation, vol. 74, John Wiley & Sons. 2009.
- [20] S. Boyd, S.P. Boyd, L. Vandenberghe, Convex Optimization, Cambridge University Press, 2004.
- [21] A. Cambini, L. Martein, Generalized Convexity and Optimization: Theory and Applications, vol. 616, Springer Science & Business Media, 2008.
- [22] H.L. Van Trees, Detection, Estimation, and Modulation Theory, Part I: Detection, Estimation, and Linear Modulation Theory, John Wiley & Sons, 2004.